Stepping through versatile attitude control system design for stratospheric platforms

STEPPING THROUGH VERSATILE ATTITUDE CONTROL SYSTEM DESIGN FOR STRATOSPHERIC PLATFORMS

Andrea Boscaleri [1], Massimo Baldi [1], Filippo Calonaci [2], Paolo Rissone [2], Federico Rotini [2].

[1] IFAC-CNR Via Panciatichi 64-50127 Florenc Italy, email: a.boscaleri@ifac.cnr.it
[2] Dipartimento di Meccanica e Tecnologie Industriali , UNIFI -Via S.Marta,3-50139 Firenze Italy, email:federico.rotini@unifi.it, email: filippo.calonaci@unifi.it, email: paolo.rissone@unifi.it

ABSTRACT

In addition to stepping through the typical hardware parts of an Attitude Control System borne for stratospheric platform, the paper describes some fast position sensors. The use of two axis magnetometers at high latitude, even though with a lower accuracy, is analyzed. A high-accuracy motorized sun tracker based on a Position Sensitive Detector photodiode capable of driving the gondola in pointing or scanning mode in any given arbitrary anti-sun direction is also presented. Lastly, as an important part of the entire sensor development project, the paper describes a simulation of the thermal behavior of a pressurized cylinder in which electronic photosensitive devices and a CPU system are housed. To employ electronic device built within a commercial temperature range and intended to stay on the ground, it is extremely important to have a pressurized and conditioned environment in order to avoid a reduction in the performances of some ACS components

1. INTRODUCTION

An IFAC team has been involved in Attitude Control System (ACS) design since the 1980s. Both mechanical and electronic parts have been continuously updated, modified and tested in several stratospheric experiments such as ARGO, TRIP, MAXIMA, BOOMERANG. The team is now extending its collaboration to BarSPOrt and OLIMPO. The ACS proposed consists of two parts: a base part, made up of an active pivot, a main computer with commercial and custom I/O boards, and a two-axes magnetometer, a second one, a set of sensors in accordance with the attitude reconstruction accuracy required. The fluxgate magnetometer can be considered as a low-cost absolute position sensor capable of orienting the platform towards a given sky sector where higher accuracy sensors such as sun trackers or star sensors can work. The magnetometer is able to show different accuracies, ranging from units of arc-seconds to tens of arc-minutes at mid or high latitude, respectively, if corrected by the declination error. Two possible scenarios at a high latitude, such as the Svalbard Islands or McMurdo station in Antarctica, are considered as border magnetometer solutions. Inside the magnetometer sector and in order to increase accuracy we propose, for high latitude, a Motorized Sun Tracker (MST) consisting of two pin-hole cylindrical shape devices with two different FOVs (4° and 60°). A two-dimensional Position Sensitive Detector (PSD) is housed in each focal plane. The PSD features a fast response photo-device and provides a continuous data position. The accuracy depends on how accurately the servo keeps the spot centered on the PSD. However, it ranges from one unit of arc-seconds to tens of arc-minutes. As a fast sensor, the sun tracker is able to drive the gondola in pointing or scanning strategies at any arbitrary area of the sky, in all of the antisun plane. It is well known that star sensors show maximum accuracy in post-processing reconstruction at every latitude. Since every platform hosts a daytime star sensor, a front-end design of a QIMAGING near infrared Camera will be displayed. A predictive MODTRAN analysis of the residual backscattered light radiance at a given antisun direction, a custom-built baffle, long-pass optical filtering and a reduced solid angle help to select which CCD is capable of detecting a given lower star magnitude.

2. THE BASE PART OF ACS

To control the movements of both the outer and inner frames of a gondola, an ACS is necessary. Centered on a CPU (we still use a robust PC104 Intel 386 and DOS 6.22) and several I/O boards, the ACS receives information from the peripheral sensors and powers the motors according to a flight program. The faster sensors take control of the motors according to a precise priority and, inside this, according to those sensors still working. Especially for Long Duration Ballooning (LDB) flights, due to the higher cost, it is extremely necessary to continue to have, in case of sensor failure, control of the gondola at all times, even if by means of the sensor with the lowest accuracy. The mechanical part of the ACS is called a pivot. This is the interconnecting point balloon-payload as in [1], and is devoted to the gondola azimuth movements. It houses two motors with high-torque sensitivity (1.4Nw.m/A) but can arrange a hollow shaft gear box to reduce

Proceedings of the 17th ESA Symposium on European Rocket and Balloon Programmes and Related Research, Sandefjord, Norway, 30 May – 2 June 2005 (ESA SP-590, August 2005)

power for fast scanning turn-around control when large inertia moments are involved. With the use of the hollow shaft gear, we aim to leave unmodified the possibility of connecting the balloon side to the onboard telemetry receiver side by means of a slip ring. A third motors drives the elevation coordinate of the telescope when scanning given patches of sky area. It is controlled by a 17-bit Encoder.

3. THE MAGNETOMETER

A flux gate magnetometer has already been successfully employed as leading main sensor in mid-latitude flights. At these latitudes, it shows a typical azimuth accuracy of tens of arc-seconds with a 10 hz bandwidth. We have explored the possibility of using the same device, but factory-adapted to the polar regions, when payloads are launched from possible known bases such as McMurdo in Antarctica or Svalbard Island in Norway. The magnetometer can be considered a low-cost, fast sensor. Once corrected for declination errors, against the influence of nearby magnetic disturbance and possible small tilt angles, the magnetometer is the first sensor through which the motors move the platform inside a given sky sector. In fig.1 we can see how the main CPU program transforms the information from a two-axis magnetometer into digital numbers that are proportional to the actual heading angle. The core of the routine features the sine (α-β) formula. Two readings from the labeled α channels are the actual heading information of the electronic compass, while the β ones are extracted from two Look Up Tables (LUT) filled at the launch base by digitizing the same magnetometer. This important operation, which is planned during the final integration phase, involves the experiment in all its parts. In a 360° compass survey and in a site far from magnetic disturbances, the gondola is either suspended under a wood crane or put on an aluminum spinning structure. In both cases, an optical encoder, in accordance with a possible azimuth resolution, triggers a 16-bit A/D converter each time that it outputs a different number. Each equally-spaced pair of numbers from the sine cosine path are stored sequentially in the LUTs labeled β. Their task is to memorize the magnetic behavior of the experiment along with each heading step. Then, when the LUTs are be transferred to the CPU memory, the flight program is ready to start. Inside each iteration, the main program reads the magnetometer quadrature signals and calls the "Tracking Converter Routine" (TCR). It returns a digital number that is free from possible coil quadrature error, from a different offset in the sine cosine paths, and from the influence of the nearby metallic mass of the experiment as well [1]. The last step is to correlate the geographical north to a digital number output from the TCR. This will be a particular point through which the true heading is referenced.

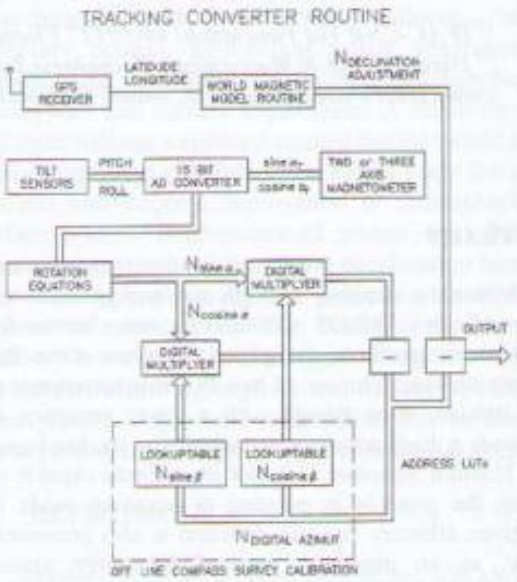

Fig.1 Tracking converter routine. It outputs a heading digital number free from all possible errors

The in-flight magnetometer performances are further improved if the readings from channels labeled "α" are corrected for any tilt of the reference sensor plane. Since gyros are always part of a high- performance pointing system, the information which they supply to the ACS can also correct this error. By applying the rotation equation, the magnetometer tilted readings can be transformed into those of the horizontal plane defined by the gravity vector as in [2].

Table 1 Horizontal magnetic amplitude variation along two possible high latitude balloon trajectories

Possible Launch Sites	Horizontal amplitude[nT]	Resolution [counts/360°]
Svalbard	7500÷500	1024
Mc Murdo	7500÷18000	8192

Fig.2 shows an example of how the main program, in a possible southern trajectory, has to correct the TCR output continuously while tracking a given target during all stratospheric flights. The same thing happens for a northern trajectory. The heading accuracy is closely related to the compass sensitivity and the amplitude of the local horizontal magnetic field (see table1).

translated by C code and inserted into the flight program. The same equation is also part of the numerator of Eq. 3. It describes the spot position error with respect to the PSD center and has an intrinsic accuracy of 1.5 arc-seconds. Fig.4 shows the result of Eq. 3 while the sun spot is kept continuously centered on the 4° FOV cylinder by the servo. Each point is displayed at a sampling rate of about 30ms . Two optical encoders arranged on the alt-azimuthal rotation axes are intended to keep track of the offset that the MST have with respect to the telescope axis. In spite of the benefit of staying in the center of the electricity, the MST loses all other information in terms of azimuth and elevation coordinates. It is easy to understand that, thanks to both the iteration time, through which the program controls the motor torque, and to the accuracy of the tracking, the MST can be labeled as a fast and accurate sensor.

$$X(Y) = \frac{L_{X(Y)}}{2} \frac{I_{X2(Y2)} - I_{X1(Y1)}}{I_{X1(Y1)} + I_{X2(Y2)}} \qquad (2)$$

$$E = \tan^{-1}\left(\frac{X(Y)}{pinhole\ focal\ length}\right) \qquad (3)$$

where:

$I_{X1(Y1)}$ = output current from electrode X1(Y1)

$I_{X2(Y2)}$ = output current from electrode X2(Y2)

$L_{X(Y)}$ = resistance length (length of the active area)

Since, like any other ACS sub-system, it must send attitude information continuously to the main CPU, the flight program can, if so required, schedule a sky sector scan centered on the actual sun position. The BarSPOrt experiment [5] will use the MST's azimuth encoder to control the amplitude and speed of any arbitrary scan, in a planned anti-sun sky sector. Fig. 5 displays the sun tracking result, along with the horizontal plane, at the earth rotation rate. However, the MST system is fast enough to accomplished a scan at a rate that is relatively higher than we can face with this kind of astrophysical experiment. BarSPOrt is planning scans at about 8-16 degrees per minute. In this case the subject of Fig. 5 will show a typical smoothed saw-tooth, instead of a line. Fig. 5 shows azimuth encoder readouts of the MST system while in Florence the servo is tracking the earth rotation. The scan deviates from the least mean square line with an error of about 7.52 arc-second RMS.

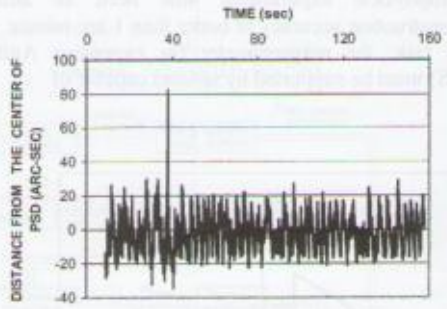

Fig.4. *Azimuth error as it comes from tan^{-1} formula (2) while the Sun Sensor is tracking the Sun Spot. The accuracy has a RMS error of about 10 arc-seconds.*

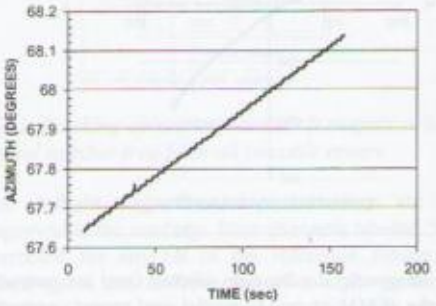

Fig. 5 Encoder readouts when the Sensor is tracking the sun's spot at the actual earth rotation rate (early March in Florence).

5.CCD STAR CAMERA

While the Sun Sensor takes advantage of both a fast loop rate and a relatively lower elevation of the sun during the high latitude summer seasons (10°-35°), the CCD star camera has the advantage of being employed at any latitude and at any time. According to the bit resolution, the frame rate, the number of pixels per frame and the optic system the CCD can be employed in different scenarios. By means of a motorized alt-azimuthal mount, the CCD can be driven to look for brighter stars independently of the actual sky patches observed [6], or it can be employed in a bore sight mount aligned with the telescope line of sight [8]. We will approach the boreside one mainly by analyzing the hardware aspect whose parameters are necessary for help in choosing between many expensive models. A bore sight camera needs to observe as many stars as possible in any sky sector both during the day and at night. During the day, identification of the stars fights

4. MOTORIZED SUN SENSOR

Astrophysical experiments now need an attitude reconstruction accuracy of better than 1 arc-minute. For this task, the magnetometer (or expensive Attitude GPS) must be supported by sensors capable of

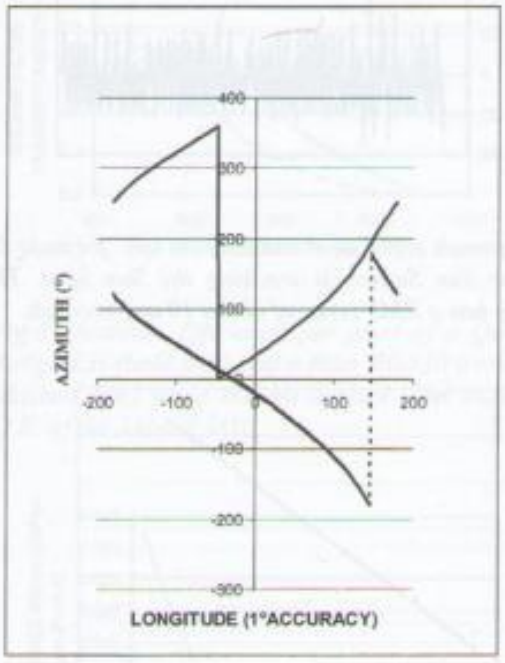

Fig.2 Magnetic declination (dotted line) as outputted from the WMM as in [3] model and target correction (bold line) necessary for pointing the same target during the entire flight

overcoming the above limit. Many research teams use a sun or a star sensor. According to their bandwidth, faster sensors are inserted in the feed-back loop, for scanning or pointing, while slower ones come into play only for data post processing. For the polar trajectory we designed a Motorized Sun Tracker (MST). It is part of the Sun Sensor class and features a faster and high accuracy sensor. It consists of two cylindrical-shape pinholes mechanically aligned in the same direction. Each cylinder has its own Field of View (FOV) of 4° and 60°, and in each focal plane it houses a two-dimensional Position Sensitive Detector (PSD) built by Hamamatsu: model S1200. Two torque motors move the cylinders by means of an alt-azimuthal mount, to try to keep the sun's spot centered on the center of the PSDs. Two absolute 17-bit encoders give the azimuth and elevation offsets with respect to the telescope's line of sight as in [4]. Remaining in the center of the electricity of the PSD gives the advantage of nullifying the variation in the dark current (see Eq. 1), and peripheral concentric zones with different accuracies never come in play. Fig 3. shows two spectral comparisons between the S1200 photosensitivity (provided by the factory) and the normalized sun irradiance simulated by MODTRAN software at Svalbard. The distance of the spectral peaks combined with the maximum current allowed make the pinhole diameter quite large (1.2 mm at float altitude). In this way, we can say that we are working far from the diffraction limit.

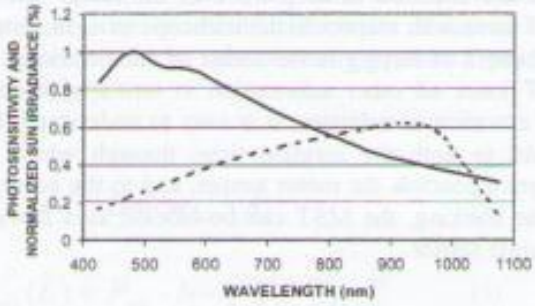

Fig. 3 Actual Spectral photosensitivity (dashed) of the irradiance at Svalbard, as predicted by MODTRAN software S1200 PSD in [A/W] compared with a normalized Sun irradiance

$$A_{ph} = \frac{I}{Bw \cdot \overline{S} \cdot \sum_{1}^{n} \overline{I}_{IRR}} \qquad (1)$$

Where:

A_{ph} = pinhole area

I = maximum current below the saturation imposed by safety criteria.

Bw = bandwidth according to the accuracy required (nm)

$\overline{I}_{IRR}$ = mean irradiance over bandwidth Bw

$\overline{S}$ = mean photo sensitivity of the PSD

n = number of bandwidth (Bw) steps

The pinhole size comes from equation (1), where we have simplified the calculation by splitting the irradiance and PSD sensitivity spectra into steps. Inside these steps, mean values of the quantities are considered. The pinhole diameter has been chosen to have a spot size able to extract electrons under the saturation current imposed (0.5 mA) by the manufacturer . The radiant power through the pinhole creates an image on the PSD surface that is able to generate photocurrent in inverse proportion to the distance between the incident spot position and each electrode. After being converted by a transimpedance amplifier and digitized by an 16 bit A/D board, the PSD's signals feature the terms of Eq. 2 . Since the MST is based on a PC104 CPU system, Eq. 2 is

with the residual sun backscattering due to the residual air pressure. Since the radiance of the scattering becomes low around after 600 nm, a camera with a Quantum Efficiency (QE) window that extends this

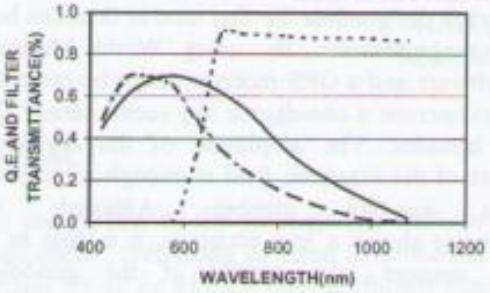

Fig.6 Quantum Efficiency per pixel of a QIMAGING Retiga Exi (bold line) and a filter RG630 transmittance (dashed line) while the dot-dashed line indicates the Q.E. of the JAI-CV M10.

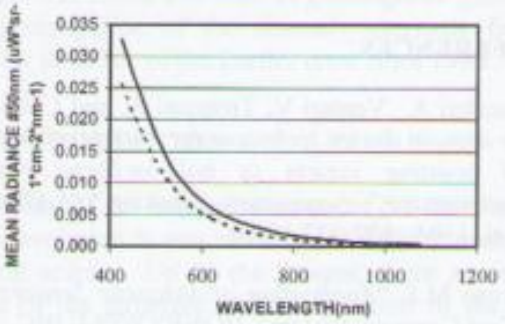

Fig.7 Spectral Radiance per pixel at Svalbard simulated by MODTRAN software. The bold line represents the backscattering with clouds and the dashed line, the one with no aerosol

limit is needed, in order to improve the SNR. The extension of the Near Infrared (NI) "tail", beyond the wavelength where the daylight scattered radiance becomes low, and the frames per second are the main aspects to consider in choosing the CCD. We focused on the Retiga Exi 1394, the Q.E. of which are displayed in Fig.6 (bold line) together the Q.E. shape for a JAI CV-M10 (dot-dashed line). It is easy to understand the differences between the two models over the red-near infrared region in terms of Q.E and of how much a difference in price (at least a ten factor) can be expected. Fig.7 shows the daytime spectral radiance at Svalbard as simulated by MODTRAN software at a balloon altitude of 40km. The sun is 120° outside the telescope's line of sight, and has an elevation of 20°. It should be noted that the Long Pass Filter (LPF) RG630, displayed in Fig. 6, greatly attenuates the residual scattered sunlight radiance that Fig.7 shows for two possible conditions below a balloon trajectory altitude: cumulus clouds (bold line) with a thickness of 3km, a visibility of 50 km at sea level, and no aerosol (dashed line). After the LPF cut-off, the rest of the NI QE efficiency is devoted to detecting stars as much as possible. Eqs.4-5 are simplified relations that combine the discrete radiance power spectrum and filter and lens performances. Obviously, the bandwidth affects the accuracy of the calculation and the photocurrent generated per pixel accordingly.

$$P_{pix} = \overline{L} \cdot Bw \cdot sr_{pix} \cdot A_L \qquad (4)$$

$$e^-_{pix}(\overline{L}) = P_{pix} \cdot N \cdot \eta \cdot \Gamma_g \cdot \Gamma_F \cdot T_i \qquad (5)$$

where:

N = number of photons/joule

P_{pix} = incident power in each pixel

$\overline{L}$ = mean radiance over bandwidth Bw

Bw = bandwidth according to the accuracy required in nm

sr_{pix} = steradiant / pixel

A_L = lens area

$e^-_{pix}(\overline{L})$ = number of electrons per pixel

η = quantum efficiency

Γ_g = glass transmittance

Γ_F = LPF transmittance

T_i = integration time

The irradiance that comes from simulation programs is not a function of the solid angle. Eqs. 4-5, without the term sr_{pix}, can also be employed when a star is observed. In the first case, they indicate the electrons generated that feature background noise; in the second one, they indicate the photo signal generated by stars. Since our lens resolution gives a spot size that is smaller than the pixel area, we consider the minimum star magnitude detectable that is capable of extracting electrons of at least 5 sigma, over 4 pixels as in [7], greater than those extracted from the residual daylight radiance. Table 3 shows possible comparison in detecting the lowest star magnitudes between CCDs by combining different commercial lenses. It is clear that to design a bore sight star camera, the RETIGA Exi, even if at the expense of a limited FOV, is the better

camera of the two models. It is a 12-bit digital monochrome device that is built around the Sony progressive scan interline sensor ICX285. The camera has its digital interface based on a fast FireWire 1394. The CPU system is centered around a PC104 400 MHz Pentium (passive cooling) that operates within a temperature range of 0°-60° Celsius. In order to avoid focus variation, the camera is kept inside its operative

Table 3 Camera comparisons versus different focal lenses

		RETIGA		JAI
Focal-f/number	Magn	FOV(deg)	Magn	FOV(deg)
135#2.8	9.2	3.8x2.8	8.3	2.8x1.9
180#2.8	9.2	2.9x2.1	8.3	2.1x1.43
200#2	8.9	2.6x1.9	7.9	1.9x1.3
400#5.6	10.0	1.3x1	9.0	0.93x0.64

range by means of a pressurized and thermally-stabilized cylinder. Pressurizing means to use fans to create turbulence in order to dissipate total power consumption (CCD plus CPU system) through surrounded internal air to cylinder and from cylinder to black body temperature of stratospheric environment. We simulated, by means of a three-dimensional program tool CosmosWorks (CM is a plug-in of SolidWorks), the transient thermal behavior and final temperature expected in the lab environment, where to the heat losses by radiation have been added the convection losses due to the presence of air. By means of a temperature sensors (AD590) two inside the cylinder and two outside in the lab environment, we calibrated a thermal predictive analysis of the CM software. The aim was to predict the flight thermal behavior of the internal environment of the cylinder in which, in addition to lenses, are arranged a commercial CPU system, built over a limited temperature range. In this way, we let the entire CCD system work properly and avoid affecting the focus of the camera. It should be noted that the LDB experiments are launched from bases located at high latitudes (Svalbard or McMurdo), and that even in the summer season the ground launch temperatures are lower than that ones expected at mid latitude base. In any case, the CCD system will be turned on only during the ascent, when the external temperature is adequate to letting the thermal control work properly.

6.CONCLUSION

The ACS for stratospheric experiments is aimed at providing the post processing with an attitude reconstruction accuracy of under one arc-minute. This goal can be achieved by means of different strategies. The star sensor is always present, and is considered to be the most accurate position sensor. We have described a simplified equation for choosing a suitable camera. But the paper also describes a high-accuracy motorized sun sensor, based on two PSDs with two different FOVs, which is able to cover a large portion of sky. It is faster than the CCD, and can also be employed for controlling arbitrary scans in an anti-sun direction. Finally, we have shown that the first sensor used to orient the gondola the first time at float can be a low-cost magnetometer. By using World Magnetic Model software and a GPS receiver, it can be corrected in order to become a one-degree sky sector sensor also at high latitudes. The amplitude of the horizontal component of the magnetic field is enough to output a consistent heading number. Although the magnetometer shows a low accuracy, it is able to let the fine sensors take control of the gondola's movements for the rest of the flight.

7. ACKNOWLEDGEMENTS

This work was supported by the Italian Space Agency under contracts N. I/R/104/02 and N. I/R/031/01

8. REFERENCES

1. Boscaleri A. ,Venturi V, Tronconi A. and Colzi R." *A time domain design technique for high precision full digital pointing system in balloon-borne remote infrared sensing*", Acquisition ,Tracking and Pointing IV , Vol. 1304 , 127-137,1990.

2. Caruso M.J. "*Application of Magnetic Sensors for Low Cost Compass System*", HONEYWELL INC.

3. National Geophysical Data Center, website URL http://www.ngdc.noaa.gov/

4. Romeo G., Debernardis P., Di Stefano G., Masi S., Piacentini F., Pongetti F.and Rao S. "*Three Sun Sensors for Stratospheric Payloads*". AIP Conference Proccedings 616, 59-61 2002

5. Balloon-Borne Sky Polarization Radiometer (BarSPOrt) Experiment http://spOrt.bo.iasf.cnr.it

6. Pascale E., Boscaleri A.,"*Attitute Control System for Balloon-Borne Experiments*", AIP Conference Proccedings 616, 56-58, 2002

7. Dietz L.K., Ramsey B., Alexander C., Apple J., Ghosh K., Swift W. "*Daytime aspect camera for balloon altitudes*", Optical Engineering Vol.41 N.10 October 2002